

Supporting Information

Influence of the Carbon Support on the Properties of Platinum-Yttrium Nanoalloys for the Oxygen Reduction Reaction

Carlos A. Campos-Roldán†, Alice Parnière†, Nicolas Donzel†, Frédéric Pailloux‡, Pierre-Yves Blanchard†, Deborah J. Jones†, Jacques Rozière†, Sara Cavaliere †^{Δ}*

† ICGM, Univ. Montpellier, CNRS, ENSCM, 34095 Montpellier cedex 5, France

‡ Institut P', CNRS - Université de Poitiers – ISAE-ENSMA - UPR 3346, 11 Boulevard Marie et Pierre Curie, Site du Futuroscope, TSA 41123, 86073 Poitiers cedex 9, France

^Δ Institut Universitaire de France (IUF), 75231 Paris cedex 05, France

*Corresponding author: Sara.Cavaliere@umontpellier.fr

* Author to whom correspondence should be addressed.

E-mail: Sara.Cavaliere@umontpellier.fr

S1. XPS deconvolution analysis

The XPS high-resolution spectra were analyzed using the Avantage software. Before fitting, a Shirley background was subtracted from raw data.

Y 3d region:

The core level Y 3d spectra were fitted using Voigt line shapes. The doublet separation was set to 2.1 eV, and the ratio between the components was set to 1.5. The Y 3d_{5/2} metallic contribution was located between 156.0 and 156.1 eV. The Y 3d_{5/2} oxide contribution, however, was proposed at 157.3 eV for Pt_xY/Cv and at 158.7 eV for Pt_xY/KB300 and Pt_xY/KB600, according to the corresponding literature, see Table S1. The peak separation between the metallic and oxide contributions has been reported to be 2.1 eV. Y₂O₃ easily adsorbs CO₂ from the atmosphere, and carbonate species were considered in the model at 157.1 eV. Table S1 presents the Y 3d peak positions used in the proposed deconvolution model of this work.

Table S1. Y 3d peak positions for the chemical species present in Pt_xY/Cv, Pt_xY/KB300 and Pt_xY/KB600.

	Peak 3d _{5/2} (eV)	Reference
Y ⁰	155.9	1 and references in it
	156.0	2
	156.0	3
Y ³⁺	158.7	1 and references in it
	158.1	2
	156.4	3
	157.4	4
Y ³⁺ -carbonate	157.7	3

Pt 4f region:

For the core level 4f Pt photoemission lines, the Voigt line shape doublets separation was set to 3.33 eV, and the ratio between the components was set to 1.33. We have considered the metallic state, the Pt²⁺ (contact with the atmosphere) and Pt⁴⁺ (chemical precursor in the synthesis) species. Table S2 presents the Pt 4f peak positions used in the proposed deconvolution model.

Table S2. Pt 4f peak positions for the chemical species present in Pt_xY/Cv, Pt_xY/KB300, Pt_xY/KB600 and Pt/C JM.

	Peak 4f _{7/2} (eV)	Reference
Pt ⁰	71.1	5
	71.2	6
	71.0	7
Pt ²⁺	72.6	5
	72.7	6
	72.3	7
Pt ⁴⁺	74.2	5
	73.1	6
	74.2	7

S2. Surface electrochemistry and ORR kinetic parameters determination

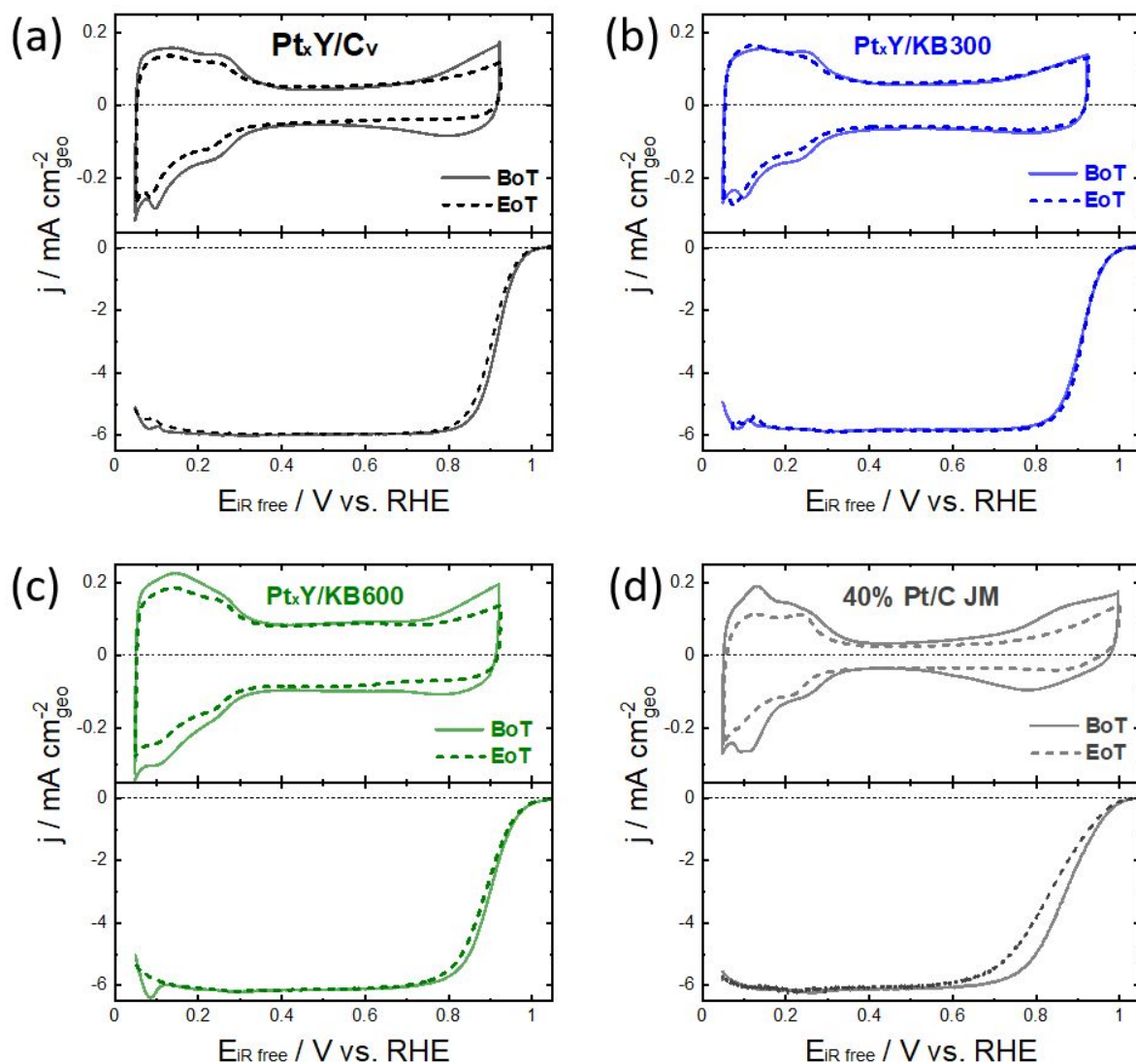


Figure S1. Cyclic voltammograms (N₂-saturated 0.1 M HClO₄ at 20 mV s⁻¹) and RDE polarization curves (O₂-saturated 0.1 M HClO₄ at 20 mV s⁻¹ and 1600 rpm) of (a) Pt_xY/C_v, (b) Pt_xY/KB300, (c) Pt_xY/KB600 and (d) Pt/C JM. Measurements were performed at BoT and at EoT.

ECSA determination

The electrochemically active surface area (ECSA) was calculated from the CO-stripping method at 20 mV s^{-1} as previously suggested for Pt-REM alloys.⁸ After the surface activation, the electrode potential was held at 0.1 V vs. RHE and CO was bubbled through the solution for 5 min. The gas flow was then switched back to N_2 for 20 min to remove the residual CO in the solution. Then, three potential cycles were performed between 0.05 - 1.0 V . Figure S2 shows an example of the obtained CO-stripping profiles.

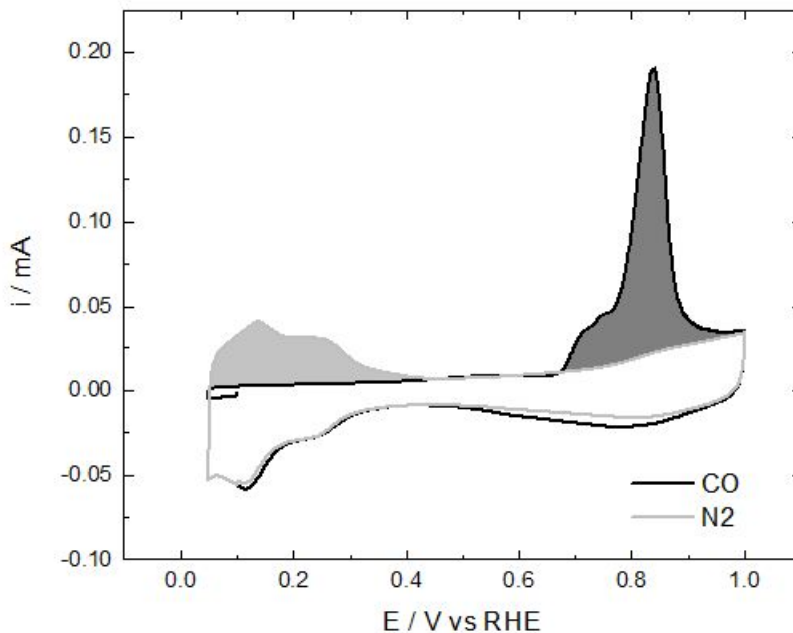


Figure S2. CO-stripping profile of 40%wt. Pt/C in 0.1 M HClO_4 at 20 mV s^{-1} .

Next, the second cycle of the experiment was used as background and was subtracted from the first cycle. The CO oxidation charge was calculated by the integration of the background-corrected curve from 0.4 - 1.0 V and its correction for the scan rate⁹:

$$Q = \frac{1}{v} \int_{0.4}^{1.0} i dE [=] \mu C \quad (1)$$

The platinum surface (S_{Pt}) was calculated assuming a theoretical value of $Q_0 = 420 \mu C \text{ cm}_{Pt}^{-2}$ for the electro-oxidation of an adsorbed CO monolayer:

$$S_{Pt} = \frac{Q}{Q_0} [=] \text{cm}_{Pt}^2 \quad (2)$$

Finally, the ECSA was derived from the normalization of S_{Pt} respect to the Pt loading (L_{Pt}):

$$ECSA = \frac{S_{Pt}}{L_{Pt} \cdot A_{geo}} \cdot \left| \frac{10^6 \mu g_{Pt}}{g_{Pt}} \cdot \frac{m_{Pt}^2}{10^4 \text{cm}_{Pt}^2} \right| [=] m_{Pt}^2 g_{Pt}^{-1} \quad (3)$$

Where $L_{Pt} = 20 \mu g_{Pt} \text{ cm}_{geo}^{-2}$; $A_{geo} = 0.196 \text{ cm}_{geo}^2$.

ORR activity determination

The ORR polarization curves were recorded by linear sweep voltammetry, from 0.05 to 1.05 V vs. RHE at 20 mV s^{-1} at 1600 rpm. The ohmic drop was determined by electrochemical impedance spectroscopy (EIS) and corrected before experiment by the potentiostat:

$$E_{corr} = E - iR [=] V \quad (4)$$

The background scan was recorded in N_2 -saturated 0.1 M $HClO_4$. Thereafter, the solution was saturated with O_2 and the polarization curves were carried out under the same conditions. Then, the background scan was subtracted from the ORR polarization curve and normalized by geometric area (c.f. Figure S9):

$$j = \frac{i_{O_2} - i_{N_2}}{A_{geo}} [=] mA cm_{geo}^{-2} \quad (5)$$

For practical purposes, the calculation was performed using the ORR current, $i_T = i_{O_2} - i_{N_2}$, rather than the ORR current density, j , (i.e. no normalization by the geometric area).

The diffusion limiting current, i_d , was obtained at the potential range where the reaction is governed by the mass-transport process (i.e. 0.4 V vs. RHE). After that, the kinetic current, i_k , was calculated through the Koutecky-Levich equation:

$$i_k = \frac{i_{dif} \cdot i_T}{i_{dif} - i_T} [=] mA \quad (6)$$

The ORR specific activity, I_s , was calculated from the normalization of i_k respect to the Pt surface S_{Pt} :

$$I_s = \frac{i_k}{S_{Pt}} [=] mA cm_{Pt}^{-2} \quad (7)$$

and the ORR mass activity, I_m , was calculated from the normalization of i_k respect to the Pt loading L_{Pt} :

$$I_m = \frac{i_k}{L_{Pt} \cdot A_{geo}} \cdot \left| \frac{A}{10^3 mA} \cdot \frac{10^3 \mu g_{Pt}}{mg_{Pt}} \right| [=] A mg_{Pt}^{-1} \quad (8)$$

S3. Raman and XPS deconvolution analysis

Raman spectroscopy

The Raman spectra were deconvoluted into five contributions with four Lorentzian peaks for the D1, D2, D4 and G bands centered around 1350 cm^{-1} , 1610 cm^{-1} , 1200 cm^{-1} and 1580 cm^{-1} respectively and a Gaussian peak centered around 1520 cm^{-1} for D3 band. The integrated

areas of D1 and G peaks were used to calculate the crystallite size L_a using the following Equation (9)¹⁰:

$$L_a = 2.4 \times 10^{-10} \times \lambda^4 \times \left(\frac{I_D}{I_G}\right)^{-1} \quad (9)$$

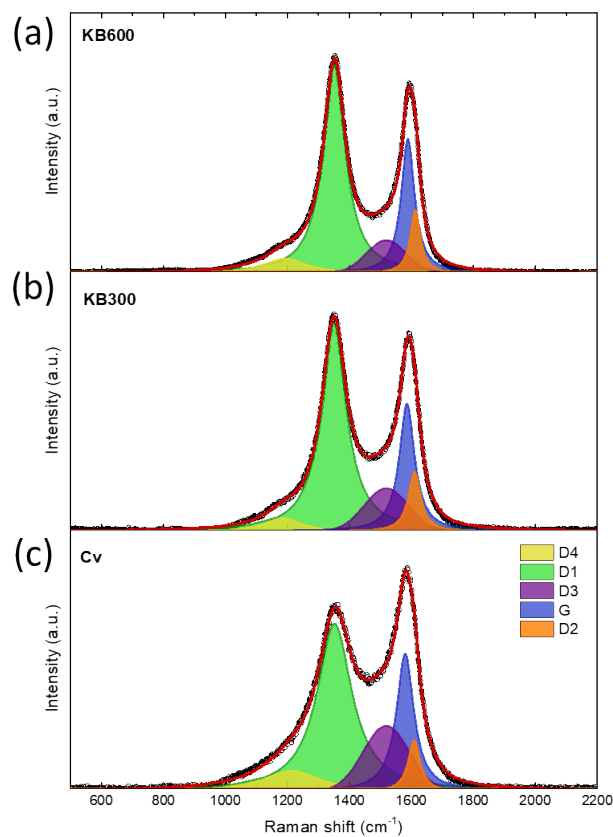


Figure S3. Deconvolution of Raman spectra of carbon supports: KB600 (a), KB300 (b) and Cv (c).

XPS

Carbon 1s region

The spectra were calibrated at 284.6 eV corresponding at the binding energy of C=C. Three contributions were used to deconvolute the C spectra at 284.4 eV, 285 eV and 286,1 eV corresponding to C=C, C-C and C-O respectively.¹¹

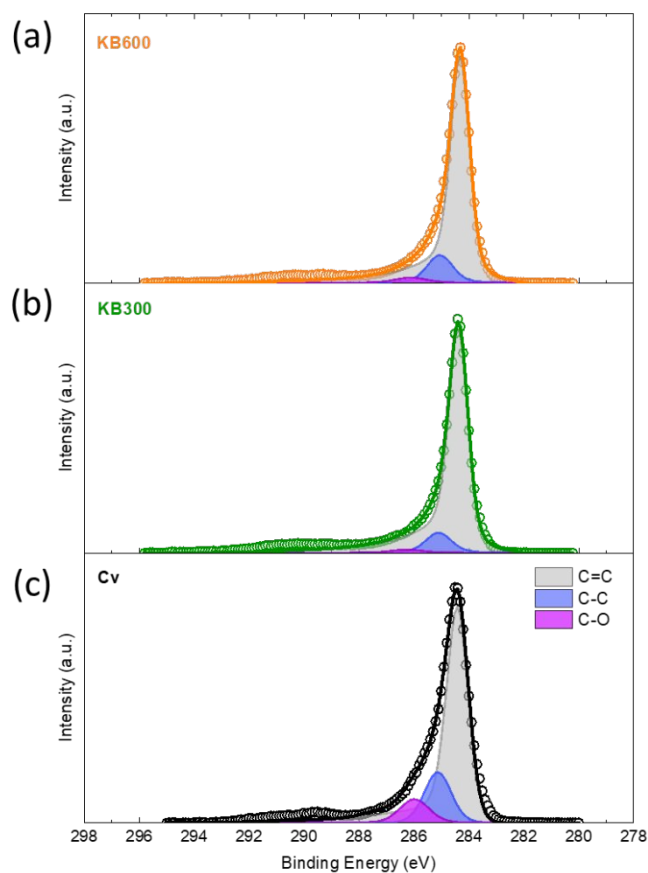


Figure S4. Deconvolution of the carbon 1s region of carbon supports: KB600 (a), KB300 (b) and Cv (c)

Table S3. Heteroatom content (%at.) determined by XPS on the surface of the carbon supports. The values determined after the Pt_xY/C synthesis are indicated in parentheses.

Carbon support	O (%at.)	N (%at.)	S (%at.)
C _v	3.37 (6.16)	0 (1.78)	0.3 (n/d)
KB300	1.51 (3.64)	0 (2.13)	0.13 (n/d)
KB600	2.60 (3.57)	0 (2.85)	0.56 (n/d)

(n/d) not determined

S4. TEM micrographs

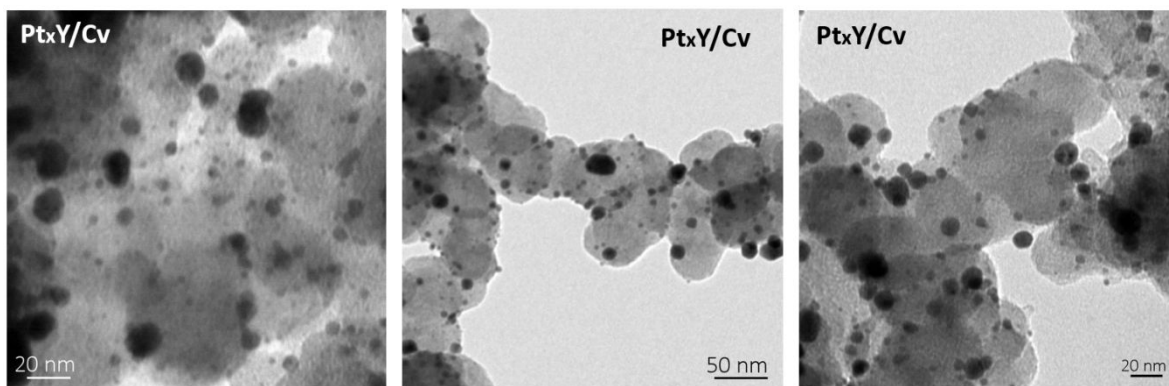


Figure S5. Representative TEM micrographs of Pt_xY/C_v electrocatalyst.

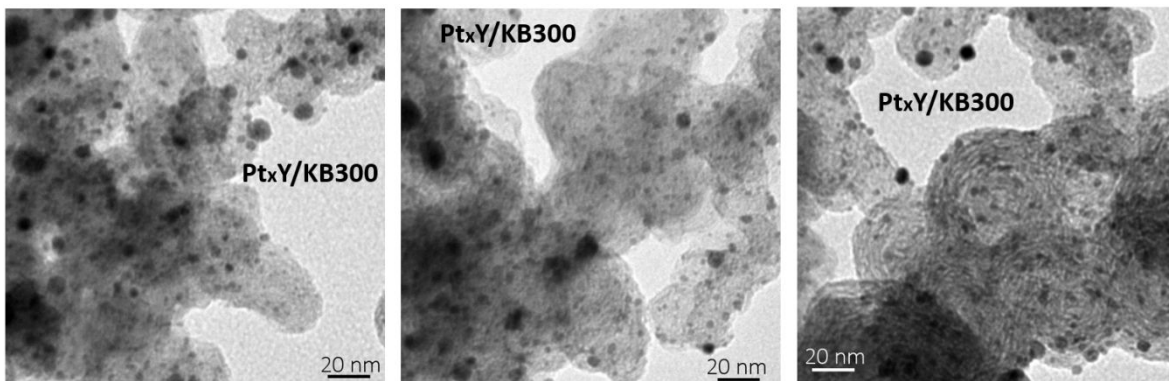


Figure S6. Representative TEM micrographs of Pt_xY/KB300 electrocatalyst.

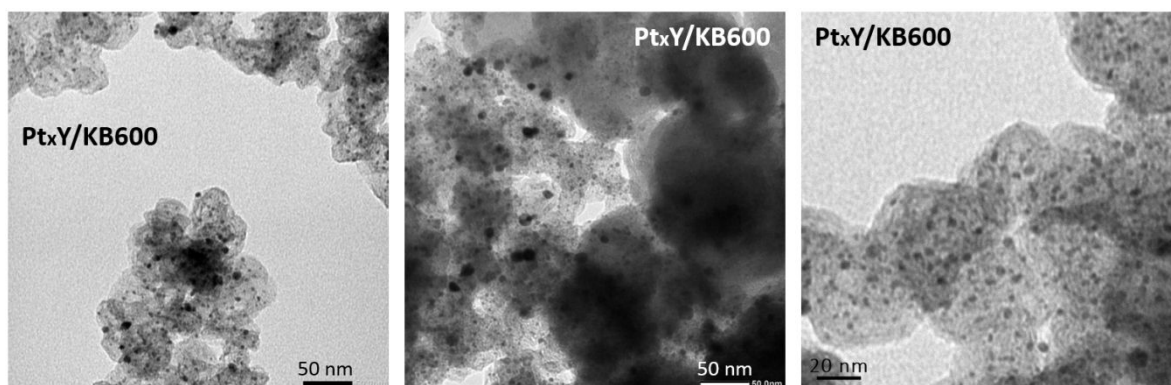


Figure S7. Representative TEM micrographs of Pt_xY/KB600 electrocatalyst.

S5. Current state-of-the-art

Table S4. Comparison of current state-of-the-art nanostructured Pt-Y alloys as ORR electrocatalysts.

Electrocatalyst	Synthesis method	Particle size (nm)	ECSA (m ² g _{Pt} ⁻¹)	I _s (mA cm ⁻² _{Pt})	I _m (A mg ⁻¹ _{Pt})	Remarks on ADT	Ref
Pt _x Y	Magnetron sputtering	9	24 n.a.*	~ 13.5 ~ 8.5*	3.05 ~ 1.09*	9000 cycles between 0.6-1.0 V in O ₂ -saturated 0.1 M HClO ₄	2
Pt _x Y/MC	Thermal reduction	4	33 n.a.*	1.57 0.90*	0.58 0.29*	10000 cycles between 0.6-1.05 V in O ₂ -saturated 0.1 M HClO ₄	12
Pt _x Y-E/C	Laser ablation in solution	Trimodal distribution (4, 18 and 48 nm)	86.1 n.a.*	0.562 n.a.*	0.48 n.a.*	n.a.	13
Pt _x Y/C	Thermal reduction	12.1	21 n.a.*	2.00 n.a.*	0.41 n.a.*	n.a.	14
Pt _x Y/C	Thermal reduction	12	14 n.a.*	0.74 n.a.*	0.10 n.a.*	n.a.	15
Pt _x Y/C	Carbodiimide complex route	~ 4.5	~ 50 n.a.*	~ 1.2 n.a.*	~ 0.60 n.a.*	n.a.	16
Pt _x Y/KB300	Carbodiimide complex route	5.2 ± 1.3 12.6 ± 1.7	61.5 53.0*	1.01 0.98*	0.62 0.51*	10000 cycles between 0.6-0.925 V in	This work

		5.9 ± 1.3* 14.1 ± 2.7*				N ₂ -saturated 0.1 M HClO ₄	
--	--	---------------------------	--	--	--	---	--

* After the accelerated degradation test (ADT).

REFERENCES

1. Malacrida, P.; Sanchez Casalongue, H.; Masinia, F.; Kaya, S.; Hernández-Fernández, P.; Deiana, D.; Ogasawara, H.; Stephens, I.; Nilsson, A.; Chorkendorff, I., Direct observation of the dealloying process of a platinum–yttrium nanoparticle fuel cell cathode and its oxygenated species during the oxygen reduction reaction. *Phys. Chem. Chem. Phys.* **2015**, *17*, 28121-28128.
2. Hernandez-Fernandez, P.; Masini, F.; McCarthy, D. N.; Strebel, C. E.; Friebel, D.; Deiana, D.; Malacrida, P.; Nierhoff, A.; Bodin, A.; Wise, A. M.; Nielsen, J. H.; Hansen, T. W.; Nilsson, A.; Stephens, I. E.; Chorkendorff, I., Mass-selected nanoparticles of Pt_xY as model catalysts for oxygen electroreduction. *Nat Chem* **2014**, *6* (8), 732-8.
3. J.F. Moulder; W.F. Stickle; P.E. Sobor; K.D. Bomben, *Handbook of X-ray Photoelectron Spectroscopy*. 1992; p 261.
4. Kenichi Kaminaga, R. S., Kouichi Hayashi, Naohisa Happo, Hiroo Tajiri, Daichi Oka, Tomoteru Fukumura, Tetsuya Hasegawa, A divalent rare earth oxide semiconductor: Yttrium monoxide. *Appl. Phys. Lett.* **2016**, *108*, 122102.
5. Campos-Roldán, C. A.; Calvillo, L.; Granozzi, G.; Alonso-Vante, N., Alkaline hydrogen electrode and oxygen reduction reaction on Pt_xNi nanoalloys. *J. Electroanal. Chem.* **2020**, *857*, 113449.
6. Singh, A.; Miyabayashi, K., Novel continuous flow synthesis of Pt NPs with narrow size distribution for Pt@carbon catalysts. *RSC Advances* **2020**, *10* (1), 362-366.
7. Kibis, L. S.; Svintsitskiy, D. A.; Stadnichenko, A. I.; Slavinskaya, E. M.; Romanenko, A. V.; Fedorova, E. A.; Stonkus, O. A.; Svetlichnyi, V. A.; Fakhrutdinova, E. D.; Vorokhta, M.; Šmíd, B.; Doronkin, D. E.; Marchuk, V.; Grunwaldt, J.-D.; Boronin, A. I., In situ probing of Pt/TiO₂ activity in low-temperature ammonia oxidation. *Catalysis Science & Technology* **2021**, *11* (1), 250-263.
8. Escudero-Escribano, M.; Jensen, K. D.; Jensen, A. W., Recent advances in bimetallic electrocatalysts for oxygen reduction: design principles, structure-function relations and active phase elucidation. *Curr Opin Electrochem* **2018**, *8*, 135-146.
9. Mayrhofer, K. J. J.; Strmcnik, D.; Blizanac, B. B.; Stamenkovic, V.; Arenz, M.; Markovic, N. M., Measurement of oxygen reduction activities via the rotating disc electrode method: From Pt model surfaces to carbon-supported high surface area catalysts. *Electrochim Acta* **2008**, *53* (7), 3181-3188.
10. Cançado, L. G.; Takai, K.; Enoki, T.; Endo, M.; Kim, Y. A.; Mizusaki, H.; Jorio, A.; Coelho, L. N.; Magalhães-Paniago, R.; Pimenta, M. A., General equation for the determination of the crystallite size La of nanographite by Raman spectroscopy. *Applied Physics Letters* **2006**, *88* (16), 163106.
11. Blume, R.; Rosenthal, D.; Tessonier, J.-P.; Li, H.; Knop-Gericke, A.; Schlögl, R., Characterizing Graphitic Carbon with X-ray Photoelectron Spectroscopy: A Step-by-Step Approach. *ChemCatChem* **2015**, *7* (18), 2871-2881.
12. Brandiele, R.; Durante, C.; Grządka, E.; Rizzi, G. A.; Zheng, J.; Badocco, D.; Centomo, P.; Pastore, P.; Granozzi, G.; Gennaro, A., One step forward to a scalable synthesis

of platinum–yttrium alloy nanoparticles on mesoporous carbon for the oxygen reduction reaction. *J. Mater. Chem. A* **2016**, *4* (31), 12232-12240.

13. Brandiele, R.; Guadagnini, A.; Girardi, L.; Dražić, G.; Dalconi, M.; Rizzi, G.; Amendola, V.; Durante, C., Climbing the oxygen reduction reaction volcano plot with laser ablation synthesis of Pt_xY nanoalloys. *Catal. Sci. Technol.* **2020**, *10* (14), 4503-4508.

14. Roy, C.; Knudsen, B. P.; Pedersen, C. M.; Velázquez-Palenzuela, A.; Christensen, L. H.; Damsgaard, C. D.; Stephens, I. E. L.; Chorkendorff, I., Scalable Synthesis of Carbon-Supported Platinum–Lanthanide and –Rare-Earth Alloys for Oxygen Reduction. *ACS Catal.* **2018**, *8* (3), 2071-2080.

15. Schwämmlein, J. N.; Harzer, G. S.; Pfändner, P.; Blankenship, A.; El-Sayed, H. A.; Gasteiger, H. A., Activity and Stability of Carbon Supported Pt_xY Alloys for the ORR Determined by RDE and Single-Cell PEMFC Measurements. *J Electrochem Soc* **2018**, *165* (15), J3173-J3185.

16. Hu, Y.; Jensen, J. O.; Cleemann, L. N.; Brandes, B. A.; Li, Q., Synthesis of Pt-Rare Earth Metal Nanoalloys. *J Am Chem Soc* **2020**, *142* (2), 953-961.